Molecular Dynamics in Cyanate Ester Resin Networks and Model Cyanurate Compounds

Benjamin D. Fitz[†] and Jovan Mijovic[*,‡]

Block Drug Company, Inc., Research and Technologies Laboratories, 257 Cornelison Ave., Jersey City, New Jersey 07302, and Department of Chemical Engineering, Chemistry and Materials Science, Polytechnic University, 6 Metrotech Center, Brooklyn, New York 11201

Received July 13, 1999; Revised Manuscript Received December 2, 1999

ABSTRACT: Molecular dynamics via broad-band dielectric relaxation spectroscopy (DRS) are obtained on a *class 3* network-forming system: a generic cyanate ester resin. The potential for in-situ monitoring of the network-forming reaction is explored. The segmental dynamics of the growing network are investigated, and a hitherto unknown secondary relaxation process, β^*, is found. This relaxation is distinctly different from the Johari−Goldstein slow β process. Model compounds and conformational strain analysis are used to elucidate the β^* relaxation molecular mechanism. The α process in selected cyanate networks was analyzed with the Adam−Gibbs thermodynamics-based relations (AG model). The AG model provides a link between the relaxation time of a cooperatively rearranging domain (CRD) and configurational entropy. The model is explored via DRS and calorimetrically for various network structures. A good agreement is found between independent quantities derived from both techniques when examined in the AG framework. These results lend support to the CRD concept used in the AG model and, more generally, toward the establishment of the heterogeneous view of relaxations in glass-formers.

Introduction

A thorough investigation of the dielectric relaxation behavior in the network-forming cyanate ester resin (general reaction scheme given in Figure 1) is absent from the literature, despite this material's widespread use in various electronics and advanced technological applications. A few examples of these applications include radar and microwave structural composites, stealth technologies, space-ware composites, circuit boards, interconnects, and adhesives for microelectronics applications (e.g., flexible and rigid die-attach adhesives). There are many features of cyanate esters that make them suitable for these technologies:[1] low dielectric constant and loss (these factors provide low wiring capacitance, low power dissipation, less cross talk, and higher signal line density),[2] low conductivity, low moisture absorption, high heat resistance (T_g > 180 °C) giving stability during soldering operations, low outgassing of volatiles, dimensional stability/low shrinkage during cure, and controlled variation of physical properties through convenient copolymerization or blending with thermoplastics.[1] Furthermore, these resins are attractive for their processing ease: low monomer viscosity, low monomer volatility, low toxicity of monomer, high purity of monomer (reproducible/reliable cure path), and favorable miscibility with thermoplastics. Another attractive property of this resin is the absence of reaction byproducts. This aspect has been taken advantage of in a recent network application involving the rearrangement of frequency addressable liquid crystalline domains within a cyanate network.[3]

Of interest here is to probe more deeply the changes in dielectric relaxation behavior in networks of systematically varied degrees of cure and to explore the potential of tailoring the dielectric properties by, for example, manipulating the network structure. From this study we anticipate learning about the more fundamental aspect of the dipole dynamics: the nature of the α-process (relaxation coupled with the glass transition) in polymers with a systematically varied network structure (degree of cross-linking).

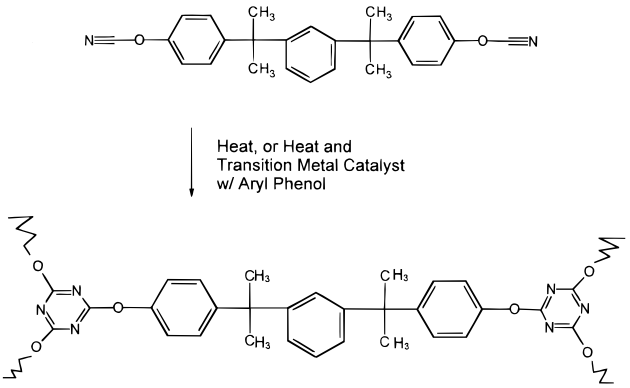

Figure 1. Structure of XU366 cyanate ester resin and reaction schematic.

In order for the dielectric relaxation spectroscopy (DRS) test to be sensitive to a network-forming polymer, there must be a permanent dipole present in the reactants and/or the products. In a recent publication[4] we have originated a classification scheme to systematize the various scenarios possible of the dipolar compositions during the formation of network polymers. Briefly, four general classes were defined. *Class 1:* dipoles present (some or all) in the reactants are not involved in the reaction. *Class 2*: dipoles present (some or all) in the reactants are involved in the reaction, and a new type of dipole is formed. *Class 3*: dipoles present in the reactants (some or all) react to form nonpolar groups. *Class 4*: nonpolar groups present (some or all) in the reactants become polar during reaction. The cyanate ester resin system under investigation here falls into class 3.

[†] Block Drug Company, Inc.
[‡] Polytechnic University.
* To whom correspondence should be addressed.

10.1021/ma9911243 CCC: $19.00
Published on Web 01/22/2000

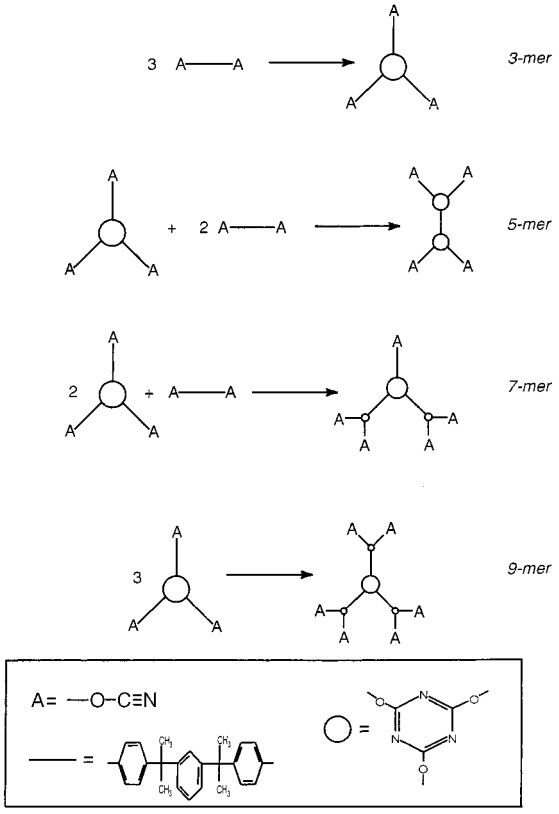

Figure 2. Structure of various reaction products (mers).

The only (to our knowledge) attempt at a dielectric study of these materials was the preliminary work of Deng and Martin.[5] Their efforts, however, were impeded by experimental difficulties: they utilized a narrow frequency range and made use of an interdigitated comb electrode geometry which yields significant electrode blocking contributions to the overall permittivity, obscuring the lower-frequency dipolar relaxations of interest during the initial low fluidity stages of the reaction. In the present work a parallel disk electrode geometry is used over a wide frequency range, and as shown in the Results section, the electrode blocking contribution does not dominate the measured permittivity.

Although there is a lack of dielectric studies on these materials, they have been well characterized by the conventional methods, the results of which we briefly summarize here. The reaction mechanism has been worked out and confirmed by FTIR and NMR on various aromatic cyanate monomers and model compounds, both catalyzed and neat.[1,6] Of interest to the present work is that although several side reactions are possible (though the dominating mechanism is direct triazine formation), they are intermediate steps to the triazine formation. Thus, our samples quenched from the reaction bath at selected degrees of cure can be assumed to consist simply of cyano groups and/or triazine groups (cf. Figure 2). The glass transition temperatures of these systems have been previously characterized by both DSC and torsional braid.[7] Our DSC measurements agree well with the previously reported glass transition temperatures. The soluble, nongelled components present at intermediate stages of reaction have been characterized by GPC (for the Bisphenol A cyanate resin),[5] and it was found that a mean-field treatment (e.g., ref 8) of the molecular weight of these solubles as a function of degree of cure is only approximate, while the following phenomenological relation for the number-average molecular weight was found to be more accurate:

$$M_n = \frac{278}{1 - {}^4/_3 \alpha k_2} \tag{1}$$

where α is extent of reaction and k_2 is a parameter, with a best fit of 0.84. The solubles have simple dendritic structures as shown in Figure 2; there is a distribution of the *n*-mers during cure, even beyond the gel point when there is a mixture of gel (infinite mer) and sol (distribution of soluble mers). Bauer et al.[9] found that the molecular weight dependence of the radius of gyration of the solubles is $0.06(MW)^{1/2}$ (in nanometers).

Theoretical and Experimental Background

Dielectric Relaxation Spectroscopy (DRS). The response of a material with permanent dipoles to an applied electromagnetic field can be written as a complex permittivity,[10,11] ϵ^* (in the frequency range where only dipole relaxations are occurring):

$$\frac{\epsilon^*(i\omega) - \epsilon_\infty}{\epsilon_0 - \epsilon_\infty} = 1 - i\omega \int_0^\infty \exp(-i\omega t)\, \phi(t)\, dt \tag{2}$$

where ω is angular frequency, ϵ_∞ is the dielectric constant at $\omega \gg \omega_{max}$ where ω is sufficiently high such that only atomic and electronic polarizations contribute (at $\omega >$ secondary β processes), and ϵ_0 is the static dielectric constant which contains the contributions of ϵ_∞ with the addition of polarizations due to permanent dipoles. $\phi(t)$ describes the polarization decay and is often modeled by eq 3, the Kohlrausch−Willams−Watts[12] (KWW) equation:

$$\phi(t) = C e^{-(t/\tau)^\beta} \tag{3}$$

where C is a constant, τ is the relaxation time, and β is a stretching exponent ranging from 0 to 1. Alternatively, $\epsilon^*(\omega)$ may be modeled by a number of empirical functions, one of which was originated by Havriliak and Negami,[13] the HN function, given by

$$\epsilon^*(\omega) = \epsilon_\infty + \frac{\epsilon_0 - \epsilon_\infty}{[1 + (i\omega\tau_{HN})^a]^b} + i\frac{\sigma}{\omega^n \epsilon_v} \tag{4}$$

where a and b are the dispersion shape parameters, σ is the conductivity, n accounts for deviations in migrating charge mechanisms, and ϵ_v is the vacuum permittivity. The other parameters are defined in eq 2.

Models of DRS Spectra. For many materials the KWW stretched exponential relaxation function,[12] eq 3, is able to satisfactorily model permittivity data. However, occasionally a more sensitive characterization of the relaxation than the KWW form is required, for example to characterize asymmetrically broadened dispersions, where, in addition to the breadth, the shape of the high- and low-frequency sides of the loss peak are needed. In this situation the KWW relaxation function is inadequate since on a log−log $\epsilon''(f)$ plot, while the slope of the high-frequency side is variable, the low-frequency side always has a slope of 1 (cf. Figure 3). Alternatively, there are two phenomenological frequency-domain models that may be considered: the Havriliak−Negami (HN)[13] function, eq 4, or that of Jonscher[14] given below. A limitation of the HN model is that for the usual limits on a and b (≤ 1), the low-frequency side in a log−

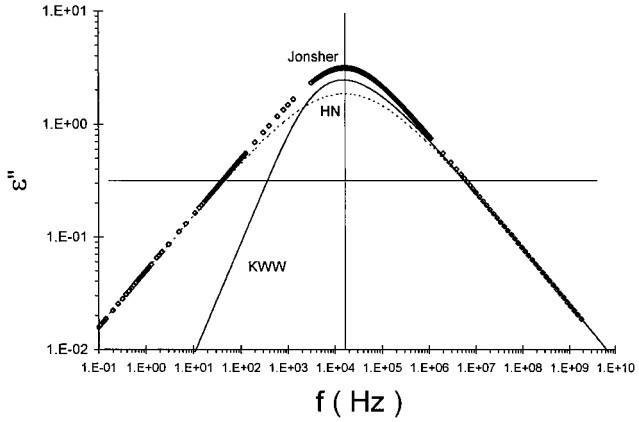

Figure 3. Comparison of KWW, HN, and Jonscher models. The parameters are KWW ($\beta = 0.5$), HN ($a = 0.5$, $b = 1$), and Jonscher ($m = 0.5$, $n = 0.5$).

log plot cannot be less steep than the high-frequency side. Either the log−log plot is symmetric or the low-frequency side is steeper than the high-frequency side. The advantage of Jonscher's power-law model is complete flexibility with regard to the high- and low-frequency slopes. Jonschers's model for the dielectric loss is

$$\epsilon''(\omega) = \frac{\Delta\epsilon_J}{(\omega_c/\omega)^m + (\omega/\omega_c)^n} + i\frac{\sigma}{\omega\epsilon_v} \qquad (5)$$

where $\Delta\epsilon_J$ is related to the relaxation strength, m is the slope in the log−log $\epsilon''(\omega)$ plot at $\omega \ll \omega_c$, n is -1 times the slope in the log−log $\epsilon''(\omega)$ plot at $\omega \gg \omega_c$, and ω_c is the peak frequency. The corresponding dielectric constant may be obtained via the Kramers−Kronig transformation of this function.[14] The HN and Jonscher models have equivalent power laws [log−log $\epsilon''(f)$ slopes] at frequencies far from the peak, but as shown in Figure 3 in the peak region, the Jonscher model (eq 5) is more narrow. The Jonscher model may be arrived at from a fundamental physical argument, from which the shape parameters gain meaning;[15] however, for the present work we do not refer to these arguments further but are simply utilizing a convenient and robust model for fitting and quantitatively characterizing the shape and breadth of the loss peak.

Experimental Section

Materials. The resin XU366 was used as received from Ciba-Geigy Corp. The monomer structure is given in Figure 1 and was confirmed by mid-infrared spectroscopy. The monomer was converted to a cross-linked network by heating either with or without a catalyst at selected temperatures (as specified below). The reactions without a catalyst were performed at an isothermal reaction temperature of 200 °C. Selected samples were prepared with a Cu^{2+} acetyl acetenoate/ in nonylphenol catalyst system at 0.2% (w/w) of monomer; further details are given in the Results section.

The extent of reaction, the fractional cyanate group conversion, has been determined in the following manner. We refer to the published data of Simon and Gillham,[16] who studied the reaction kinetics on the same uncatalyzed cyanate ester resin system. They determined the extent of reaction via in-situ mid-IR. They found a strong correlation between DSC T_g and conversion determined by IR; moreover, at high conversion, the DSC T_g was more sensitive to conversion than the IR measurements, since in the later stages of reaction the largest changes in T_g are found. The relation between T_g and conversion for this system is nonlinear and may be derived

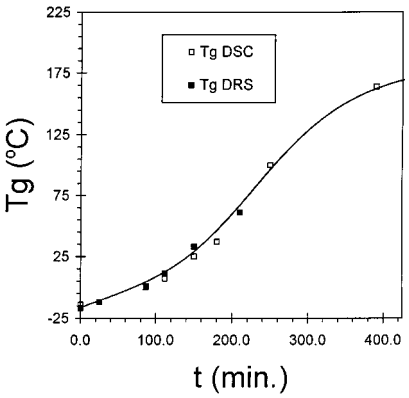

Figure 4. Glass transition temperature (via DRS and DSC measurements, see text for details) as a function of isothermal reaction at 200 °C.

from thermodynamic considerations[17] and is written

$$\%\ \text{rxn} = \frac{\ln T_g - \ln T_{g0}}{\frac{\Delta C_{p\infty}}{\Delta C_{p0}}\ln T_{g\infty} - \ln T_{g0} + \ln T_g\left(1 - \frac{\Delta C_{p\infty}}{\Delta C_{p0}}\right)} \qquad (6)$$

where T_{g0} is for the 0% resin, $T_{g\infty}$ is the T_g of the 100% reacted material, and ΔC_{p0} and $\Delta C_{p\infty}$ are the heat capacity increments at T_{g0} and $T_{g\infty}$, respectively. An additional finding of Simon and Gillham[16] is the independence of reaction temperature on T_g at a given extent of conversion. Thus, once the parameters (right-hand side of eq 3: $\Delta C_{p\infty}/\Delta C_{p0} = 0.38$, $T_{g0} = -16$ °C, and $T_{g\infty} = 177$ °C) are obtained for this particular cyanate ester resin, a simple T_g measurement may be used to obtain the extent of reaction. We rely on this relation to determine the extent of reaction for our uncatalyzed reaction at 200 °C. We present our calorimetric findings of the DSC T_g values as a function of isothermal reaction time in Figure 4. (The samples were obtained as quenched aliquots from an isothermal reaction at 200 °C.) The solid curve through the data is a phenomenological fit we are introducing to calculate the T_g at any isothermal reaction time:

$$T_g(t) = \frac{T_{g\infty} - T_{g0}}{1 + (A/t)^n} + \frac{B}{(t/A)^m + A/t} - T_{g0} \qquad (7)$$

where $A = 270$ min, $T_{g\infty} = 177$ °C, $T_{g0} = -16$ °C, $n = 4$, $m = 2$, and $B = 60.13$ °C. The experimental T_g values are then used, and the corresponding extent of reaction is calculated using eq 6.

Dielectric Relaxation Spectroscopy. A detailed description of our experimental facility for dielectric measurements is given elsewhere.[18] However, briefly, we have used a Solartron 1260 impedance/gain-phase analyzer to cover the frequency range 10^{-3} Hz to 10 MHz. This analyzer was used in conjunction with a high-impedance adapter of variable gain and a high-precision heating and cooling chamber, both from NOVOCONTROL. From 1 MHz to 1.8 GHz an HP4291A impedance analyzer was used in conjunction with a sample cell, high-precision extension air-line, and calibration software from NOVOCONTROL GmBh. An HP8752A network analyzer was used for the range 10 MHz−1.3 GHz, making use of our own modified sample cell and software to calculate the complex dielectric constant from the measured reflection coefficients.

Differential Scanning Calorimetry. The calorimetric work presented herein was performed on a TA2920 DSC with an average sample size of 10 mg. All heating rates were 10 °C/min. We have used the TA Instruments 2920 DSC in nonmodulating mode. As this instrument has a notably steady and reliable baseline, we have converted the measured heat flow to a C_p*, a qualitative heat capacity. This conversion suited our interest in obtaining qualitative configurational entropy values. The C_p* values are then simply the measured heat flow (in W/g) multiplied by dT/dt divided by sample mass

and converted to joules. We emphasize that these derived C_p* values remain qualitative since no C_p calibration steps were taken; however, the error in the heat capacity change at the glass transition for this instrument is reported as <5%.[19]

Dynamic Mechanical Analysis. A Rheometrics DMTA dual cantilever beam DMA was employed. The resin was cast and cured in a mold of rectangular sample geometry: 1.34 mm × 12.84 mm × 7.00 cm. A 95% reacted sample was scanned from −100 to 250 °C using 0.3, 1, 3, 10, and 30 Hz frequencies.

Wide-Angle X-ray Scattering. We employed a Siemens Hi-Star diffractometer. The wavelength used was Cu Kα at λ = 1.542 Å, with a collimator of 0.5 mm. The samples were contained in glass capillaries; the diffraction pattern of the empty capillaries were subtracted from the experimental sample patterns.

Results and Discussion

Dynamics by DRS: In-Situ Chemical Changes vs Selected Isostructural Networks. Our DRS study consists of two approaches: (1) in-situ isothermal measurements, allowing us to assess the capability of DRS to monitor network formation in real time in this class 3 network-forming system, and (2) samples at selected extents of reaction quenched from the reaction bath and measured across a wide range of temperature (from below T_g and up) and frequency. It is important to note that the samples measured at selected conversions (quenched samples) do not react further during subsequent measurements, as the uncatalyzed material has a very low reactivity at temperatures less than 150 °C. This approach allows us to characterize the dipolar relaxation dynamics of selected reaction products, selected network connectivity, polarity, and molecular size distribution. We present the quench/reheat data first.

Molecular Dynamics In Stable Rigid Networks: Approach 2 (Quench/Reheat). The most direct and convenient illustration of molecular dynamics (via dipoles) is in the form of a dielectric loss spectrum, $\epsilon''(f)$, where the shape and peak frequency (reciprocal of the α apparent relaxation time) are immediately seen. Thus, we present this form of experimental dielectric data in Figure 5 for the neat resin (0%) and samples of 20, 30, and 40% conversion. These data are collected for the α process at temperatures near and above T_g. We summarize the interesting features of these plots. All of the samples exhibit a temperature dependence of the shape of the loss peak. The general trend is that the low-frequency flank of the peak rises with decreasing temperature, and this effect is enhanced with increasing conversion. The temperature and extent of conversion dependent change in the low-frequency side of the loss peak has four possible explanations: (1) an artifact due to conductivity/electrode effects that is not a feature of the α process itself; (2) an unusual temperature dependence of a *continuous distribution* of relaxation processes (heterogeneous scenario);[20] (3) an unusual temperature dependence of two, or perhaps three, *distinct* relaxation processes (also heterogeneous scenario);[20] or (4) an unusual temperature dependence of an asymmetric broadening phenomenon in a relaxation process that is inherently broad (*no distribution*) (homogeneous scenario).[20] The first possibility may be eliminated by a reexamination of the data. We have replotted the loss data in Figure 6 at the convenient temperature of 50 °C, so that their shapes may be compared more easily. Since these relaxations are at the same temperature, the effects of thermal agitation on the dielectric relaxation strength are equivalent.

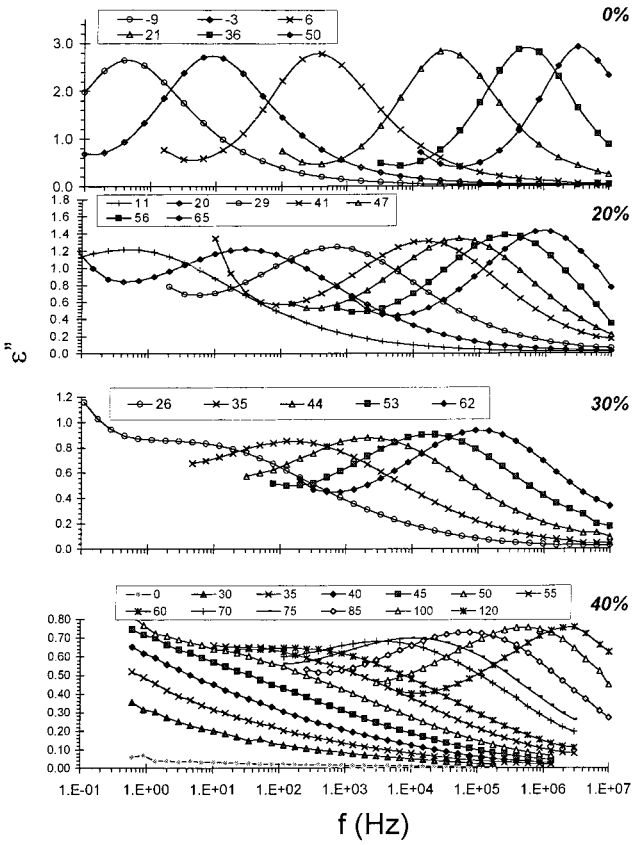

Figure 5. Dielectric loss as a function of frequency at 0, 20, 30, and 40% conversion, with temperature as a parameter.

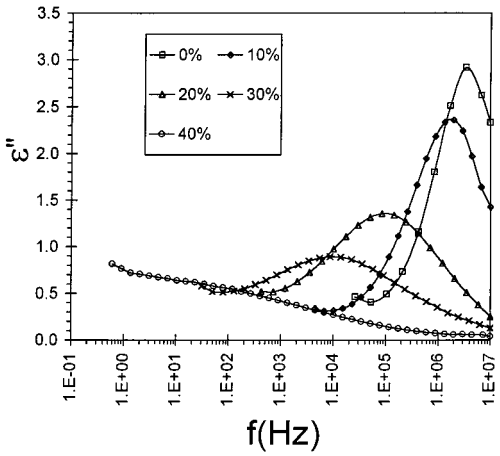

Figure 6. Dielectric loss as a function of frequency for 0, 10, 20, 30, and 40% samples at 50 °C.

At 50 °C (at thermal equilibrium) while the average thermal kinetic energy, $^3/_2kT$, is equivalent for all of the samples, their relaxation times are different. Simplistically, we can say that this is due to their different T_g's. Microscopically, the mobility of the medium surrounding a given dipole is reduced with increasing T_g. We are assuming that the only active dipoles in this material are the cyanate groups (at the low temperatures of these measurements this is a fair assumption).[6] The fundamental mobility (*primitive segmental* mobility) of a given cyanate dipole is determined by the *inherent* activation energy for torsional rotation around the two bonds between the phenyl and cyano oxygen (cf. Figure 7). Since the linear −O−C≡N is conformationally fixed, and the torsional rotation around O−C is dielectrically inactive, the only major motion of this molecule observ-

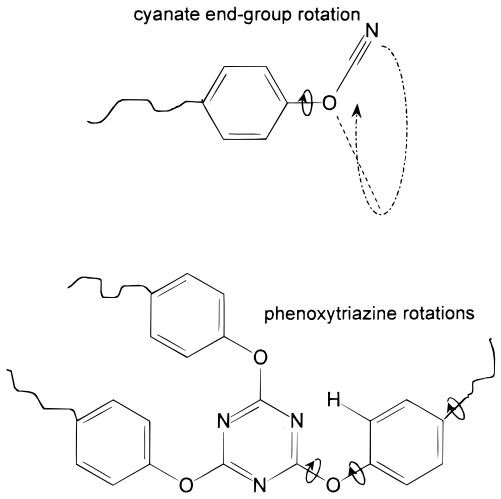

Figure 7. Illustration of dipolar mobility in cyanate resin and in triazine structures.

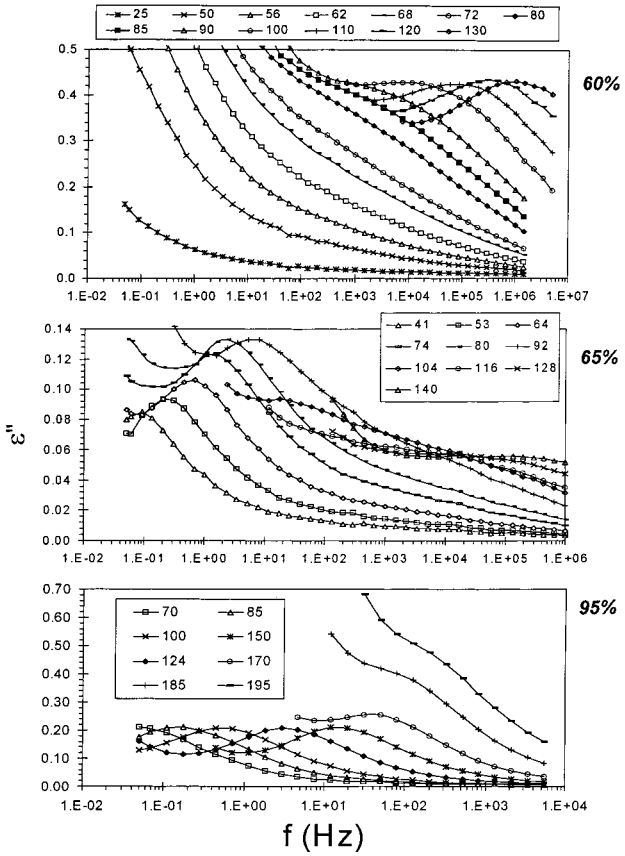

Figure 8. Dielectric loss as a function of frequency at 60, 65, and 95% conversion, with temperature as a parameter.

able with DRS is the torsional rotation around the Ph−O bond (Figure 7). This rotational mobility (energy barrier) is independent of cross-linking, i.e., independent of any chemical reaction on the other side of a given monomer molecule (cf. Figure 1). The *actual*, bulk, Ph−O activation energy is a combination of the above intramolecular interaction barrier and intermolecular interactions with the surrounding media (composed of aromatic, isopropyl, triazine, and cyanate groups). At an extent of reaction of approximately 64% a macroscopic network is formed. At this point many of the intermolecular interactions are permanent and physical, in contrast to lower extents of conversion, where the interactions are temporal. The result is the sudden qualitative change in the dielectric loss spectra above 60% reaction (cf. Figure 8, 95% sample) and the emergence of a new relaxation process termed β*, which is considered next.

Anomalous Secondary Relaxation: *β**. The β* process is active below the glass transition temperature, with a linear (Arrhenius) relaxation time temperature dependence. Its activation energy is ~80 kJ/mol (~20 kcal/mol); the prefactor is $\sim 10^{-13}$ s. This process is sensitive to T_g (though indirectly), as its τ at a given temperature is higher with increasing T_g. The shape of this process is less broad than many other sub-T_g β processes (the usual Johari−Goldstein[21] slow β processes); we have found that its shape is best fit with a KWW β parameter of 0.59 (note that "usual" secondary β processes are much more broad, having KWW β parameters between 0.1 and 0.3).[18] The molecular origin of this process is evidently the phenyl−triazine ether linkages. We have made this deduction based on the fact that a strikingly similar β process exists in three phenyl−triazine linkage-containing materials. These materials are (1) the fully reacted XU366 resin, (2) a similar resin, also fully reacted (recall that triazine formation increases with cure, so that a "fully reacted" material will have its maximum triazine content), with the trade name Arocy B10, supplied by Ciba Geigy, whose monomer structure is

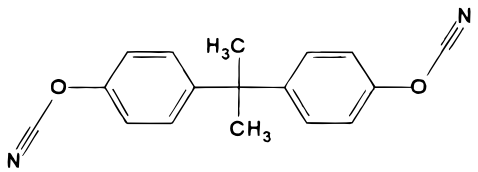

and (3) a low molecular weight model compound, 1,3,5-triphenoxy-2,4,6-triazine (99%, Aldrich, mp 232−235 °C) hereafter referred to as TPT. Its molecular structure is

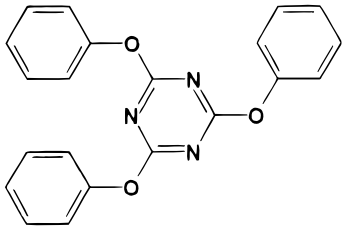

Note that TPT has an identical structure to the structure of the network junctions in XU366 and B10, and furthermore it is highly crystalline (~99%), the three-dimensional order in the crystal resembling the semi-ordered constraints of its network-forming "cousins". The similarities in dielectric response between the β* processes in the fully cured XU366, B10, and the crystalline TPT response are (1) same activation energy within experimental error, 80 ± 2 kJ/mol (20 kcal/mol), (2) same shape (characterized for example by KWW β of 0.60), and (3) same temperature dependence of the dielectric relaxation strength, $\Delta\epsilon$. Coincidentally, the values of activation energy for this β process are similar to those of the α_c processes in the semicrystalline polymers: poly(vinylidene fluoride), 23 kcal/mol;[22] and polyethylene, 21 kcal/mol.[23] A concise table containing the β* Arrhenius parameters is given in Table 1.

A question arises: although we may associate the β* process with the triazine moiety, can we assign a more specific molecular motion? The possibility of specific

Table 1. Arrhenius Parameters for β* Processes

material	E_a (kJ/mol)	E_a (kcal/mol)	log τ_0
TPC, crystalline	83.3	19.9	−12.9
B10 100%, annealed	96.3	23.3	−12.8
B10 100%, quenched	88.4	21.1	−12.1
XU366 100%, neat	88.8	21.2	−12.8
XU366 100%, with catalyst	90.4	21.6	−13.93

assignment seems reasonable since the relaxation is occurring within a highly constrained moiety; hence, we may make plausible assumptions on the locations of selected portions of the triazine. We have undertaken a conformational analysis of total internal strain using the commercially available software package, ChemSite 2.42 by Pyramid Learning LLC, 1998. Our use of the software was the following. First a simpler, but representative, model of a phenoxytriazine was created:

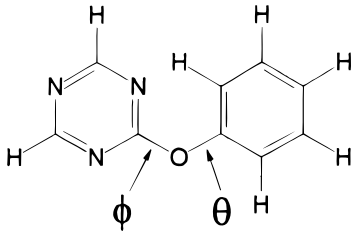

This structure conformation was minimized using the software's AMBER minimizer, which periodically quenches the molecular dynamics to minimize energy. The conformation shown above is that of the highest strain energy and illustrates the torsional bond angles ϕ and θ (0° for both angles shown). The conformational analysis consisted of the following procedure. First, ϕ was set to 0°, and the θ torsional bond angle was varied by 0.5° from 0° to 360° while the total strain energy was continuously collected. (The software considers steric, 6−12 Lennard-Jones, and H-bonding interactions when computing strain energy.) As the barrier between θ of 90° and 270° is very large (3000 kcal/mol), the average conformation of this bond must generally be near 90° or 270°. Applying this finding, we next set the θ angle to 90° and ϕ was varied between 0° and 360°. The barrier for rotation between 90° and 270° is ∼7 kcal/mol. We then replaced the model triazine with TPT (structure given previously) in ChemSite and found that the barrier energies were nearly equivalent to those of the model compound. For three phenoxy rotations around the three θ bonds a value of ∼21 kcal/mol is found; the agreement with the DRS β* activation energy and this strain barrier suggests that the origin of the β* process is a cooperative flip of three phenoxy groups. Solid-state NMR is indicated to confirm this finding.

A second question arises: why is this process not observed in the samples with conversion lower than 65%? There are two explanations. The first explanation holds until approximately 40% conversion. It is that there are simply very few phenoxytriazines present in the early stages of cure, but even when their numbers grow with increasing reaction, since the relaxation strength for this process is ∼10 times smaller than the α process, it remains too small to be detectable. The second explanation holds for conversions above 40%. In this situation the β* process is hidden by the large conductivity/electrode effects which contribute at low frequencies; however, when the system gels at 64%, the conductivity is drastically reduced, the main α relaxation strength has decreased sufficiently, and the process is observable.

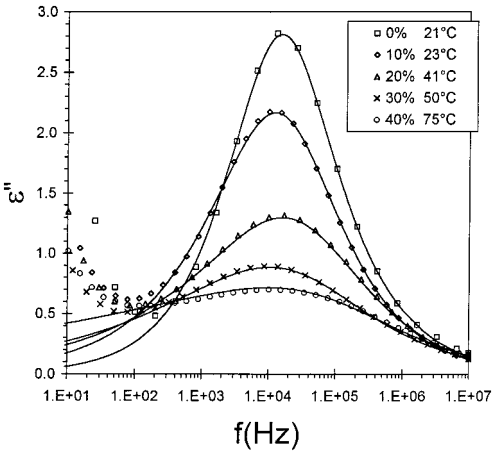

Figure 9. Dielectric loss spectra for 0, 10, 20, 30, and 40% samples at an "isomobility" temperature (temperature where the frequency of ϵ''_{max} is 10^4 Hz). Solid lines are fits to the Jonscher model, eq 5; the parameters are given in Table 2.

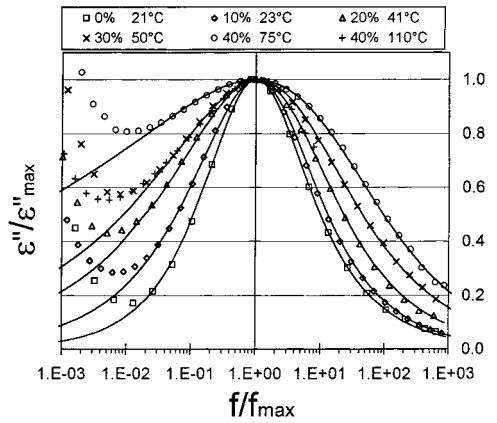

Figure 10. Normalized dielectric loss spectra for 0, 10, 20, 30, and 40% samples at an "isomobility" temperature (temperature where the frequency of ϵ''_{max} is 10^4 Hz). The solid lines are fits to the Jonscher model.

Broadening of the α Process during Network Growth. As conversion increases, the α process appears to broaden, while its intensity decreases. It is well-known that the loss shape can be temperature dependent. To assess the influence of a temperature-dependent change of shape on the increasing breadth of the α process, we replot the data at an "isomobility" temperature, i.e., at a temperature where the process has a convenient loss maximum of 10^4 Hz. These plots are shown in Figure 9 (raw data), and the normalized spectra are shown in Figure 10, illustrating that with increasing conversion the α loss peak indeed becomes more broad, although, as shown by the 40% sample at an elevated temperature, this peak shape is quite temperature dependent, narrowing with increasing temperature. The temperature dependence may be further examined. The width of the peak (in decades of frequency) at half of the peak height is a common measure of the breadth of a relaxation distribution.[10] We show these data in Figure 11 for samples of 0, 20, and 40% and for the sample undergoing isothermal reaction at 100 °C. This figure shows that although the peak shapes are narrowing with increasing temperature, with increasing conversion there is a significant

Table 2. Jonscher Power-Law Fit Parameters and HN Model Parameters for Samples at Selected Extents of Reaction at an "Isomobility" Temperature: the Temperature at Which the Frequency at ϵ''_{max} Is 10^4 Hz

	Jonsher parameters					HN parameters			
% rxn	T (°C)	$\Delta\epsilon_J$	τ_J (s)	m	n	$\Delta\epsilon_{HN}$	τ_{HN} (s)	a	b
0	21	5.62	1.14e−5[a]	0.62	0.55	9.5	1.7e−5	0.77	0.69
10	23	4.30	1.00e−5	0.43	0.55	8.8	8.8e−6	0.51	1.27
20	41	2.51	5.06e−6	0.29	0.49	6.7	5.7e−6	0.43	1.38
30	50	1.70	6.13e−6	0.23	0.42	5.3	7.5e−6	0.38	1.38
40	75	1.17	1.24e−6	0.11	0.43	5.2	6.2e−6	0.23	4.56
40	110	1.44	4.81e−8	0.23	0.49	4.6	11.1e−8	0.32	2.34

[a] Read as 1.14×10^{-5}.

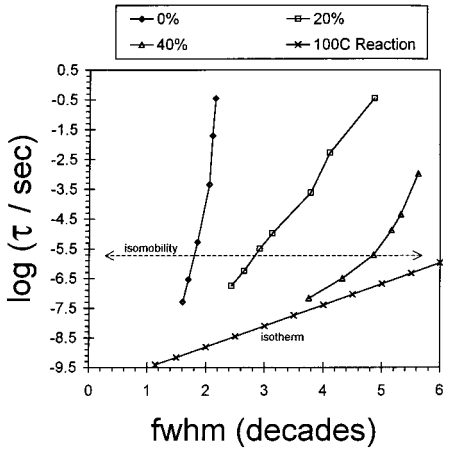

Figure 11. Width of the dielectric loss peak (in decades of frequency) at $^1/_2$ of the maximum intensity (abbreviated fwhm) for selected samples: 0, 20, and 40% and as measured during isothermal reaction at 100 °C (showing the increasing peak breadth with conversion).

increase in breadth that may not be overcome by comparing relaxations under "isomobility" conditions. (The "isomobility" conditions in Figure 11 are a set of temperatures where the peak maxima coincide; this condition may be found by creating a horizontal line from a given log τ in the figure.) From Figure 8 it is also clear that there is not a significant influence from conductivity in the frequency region near the loss peak. Both of the foregoing analyses lead us to conclude that the broadening is a real feature of the relaxation itself.

The shape of the peaks in Figure 10 are characterized and quantified by the Jonscher model (eq 5); the parameters are given in Table 2.

The Jonscher parameters $m = 0.62$ and $n = 0.55$ for the neat resin are comparable to those of many polymers and low molecular weight materials; however, with increasing conversion both parameters decrease, but the m parameter becomes smaller than n. This behavior is unusual. In Jonscher's monograph[14] where the parameters are given for 65 different materials, only 18 have smaller m's than n's. The broadening trend of the α process with cross-linking is not a new finding;[24,25] precisely why the broadening occurs remains unclear. Previous work on epoxide/amine cross-linking systems has quantified the α peak shape with Jonscher parameters of m ranging from 1.0 to 0.55 and 0.5 to 0.13 for n during cure.[26−28] For a cross-linking urethane system m ranged from 0.86 to 0.4 and n from 0.4 to 0.15.[29,30] For both the epoxide/amine and urethane systems mentioned above, at no time during cure were the m parameters less than the n parameter; this behavior seems to be unique to the cyanate system.

Another interesting feature of these cyanate networks is the following. For the 0% resin, based on the temperature-dependent positions of the peak maxima and adjacent low-frequency sides of peak minima (of Figure 5), the neat (0%) resin's dipolar movements exhibit the same temperature dependence as the conductivity. While for 10, 20, 30, and 40% samples the dipolar relaxation peak temperature dependence (dipolar mobility) is greater than that of the conductivity. This behavior is most apparent in the 40% sample, where at low temperatures the α process is obscured beneath the conductivity contribution, but with increasing temperature the α peak shifts up to higher frequencies with increasing temperature more quickly than the conductivity increase. The significance of this interesting finding is unclear at present.

Next we offer two interpretations of the broadening of the α process. First is broadening due to microscale composition variations (concentration fluctuations). Such broadening phenomena have been studied for polymer blends using the DRS technique by Katana et al.,[31] who studied the binary blend of (Bisphenol A polycarbonate, BPAPC/tetramethyl Bisphenol A polycarbonate, TMBAPC) and found a maximum in the broadening of the α process at ∼40 mol % of TMBAPC but, interestingly, found no difference in ΔT_g (temperature range of calorimetrically determined glass transition) or $\Delta C_p(T_g)$ (extrapolated heat capacity difference between liquid and glass) for these blends, and Kumar et al.,[32] who developed a mathematical model based on nanoscale concentration fluctuations, predicting a broadening of ΔT_g and width of the α process for miscible polymer blends. Arguments along similar lines have been set forth by Roland and Ngai,[33] though they refer to the phenomenon generically as heterogeneous broadening. We acknowledge that a small contribution to the broadening in our cross-linking system is due to these compositional fluctuations; however, it is apparent that the severity of the broadening for our network's α process must have an additional explanation.

We have shown in a previous publication[4] that the breadth of the α process in a polymer network is unchanged when the distance between cross-links is greater than the length scale of the cooperatively rearranging domain (CRD). In the present network, consisting of rigid cross-link nodes and rigid sections connecting those nodes, we propose that the CRD is relatively large and on the order of (or larger than) the distance between cross-links (∼18 Å, see Figure 1). In this case the α dynamics will become increasingly disturbed and heterogeneous with the progress of cross-linking, with an ultimate disappearance of the α process in perfect networks of this kind. We assert that this influence on broadening the α process is greater than the influence of concentration fluctuations mentioned above.

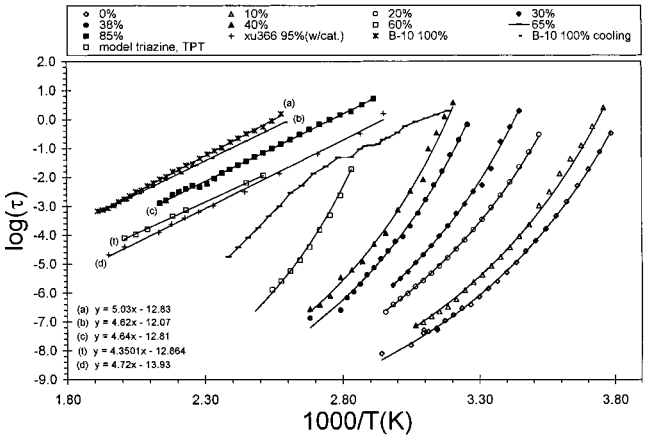

Figure 12. Log τ vs 1000/T (K) for selected samples indicated in the figure.

Table 3. VFT Parameters Obtained from DRS Measurements on Samples at Selected Extents of Reaction

min at 200 °C	T_g(DRS) (°C)	% rxn	E_a (eV)	T_v (°C)	T_v/T_g
0	−17	0	0.14	−63	0.82
25	−12	10	0.15	−61	0.81
87	1	20	0.18	−55	0.80
112	11	30	0.17	−44	0.81
150	33	40	0.18	−24	0.81
210	61	60	0.18	5	0.83

Relaxation Strength of the α Process. Although the loss peak maximum increases with temperature for all samples up to 40% (for peaks observed in the frequency regime: 1×10^{-2} to 1×10^{7} Hz), the relaxation strength obeys the 1/T Curie law temperature dependence. The Curie law dependence indicates that the relaxing −OC≡N dipolar motions are not correlated.

Temperature Dependence of τ_α. The temperature dependence of τ for samples at selected extents of reaction is given in Figure 12. The solid lines in this figure are best fits of the data to a Vogel−Fulcher−Tammann[34] function; the parameters are displayed in Table 3. The VFT equation is defined as

$$\tau = \tau_0 \exp\left[\frac{E_a}{k(T - T_v)}\right] \qquad (8)$$

where τ_0 is the high-temperature−high-frequency limit for τ, E_a is an apparent activation energy for the process, k is the Boltzmann constant, and T_v, the Vogel temperature, is a temperature below T_g where the relaxation is considered to be frozen. The DRS T_g (shown in Figure 4) is obtained from the VFT fit: $T_{gDRS} = T_v + E_a/k^*(\tau_0 - \tau_{T_g})$. (By convention, T_g is taken to be the temperature at which the segmental relaxation time is 10^2 s.) A striking change in log $\tau(T)$ occurs for samples >60% conversion (recall that the gel point of this system is ∼64%[16,35]). The T_g/T scaled "fragility"[36] plot is shown in Figure 13 for 0 and 38% samples. There is no significant difference in fragility between these samples. At present there are no unambiguous quantitative relations between molecular structure and fragility; thus, we hesitate to offer an interpretation.

Isothermal Cure Monitoring. A selected isothermal DRS measurement during cure is shown in Figure 14, where the dielectric loss is shown as a function of frequency at the given cure times. At this cure temperature the maximum degree of conversion is ∼70%. The T_g at infinite time at this isothermal reaction temperature is ∼105 °C. This figure shows that at 100 °C the material is initially liquidlike (relaxation time of ∼800 ps) and has a "normal-looking" α process. With increasing reaction time the α process broadens (as verified in Figure 11) and slows down. At 450 min of reaction the α process occurs at frequencies where conductivity/electrode effects dominate; beyond this extent of reaction the material no longer has an identifiable α process. At the completion of this isothermal experiment (the time at which no further dielectric changes were observed), the sample temperature was raised to 225 °C for 25 min for postcuring and was then cooled at 10 °C/min to 100 °C. The dielectric loss for this postcured sample is given in Figure 14. As discussed above, since the material is at 100% conversion, the β* process is now evident. The temperature dependence of the relaxation time for this process is shown in Figure 12. This β* process has a lower log τ_0 than the others because this material has the lowest T_g. The lower T_g is due to the presence of the catalyst carrier moieties (nonylphenol and acetyl acetenoate), which are present in dielectrically undetectable levels but act as plasticizers on the network. ($T_{g\infty}$ of the catalyzed network is ∼155 °C, vs 175 °C for the uncatalyzed network.)

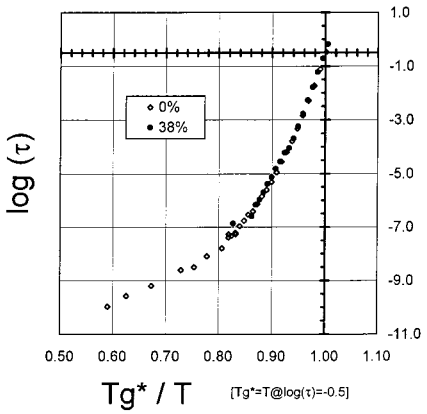

Figure 13. Log τ vs T_g/T for 0 and 38% samples.

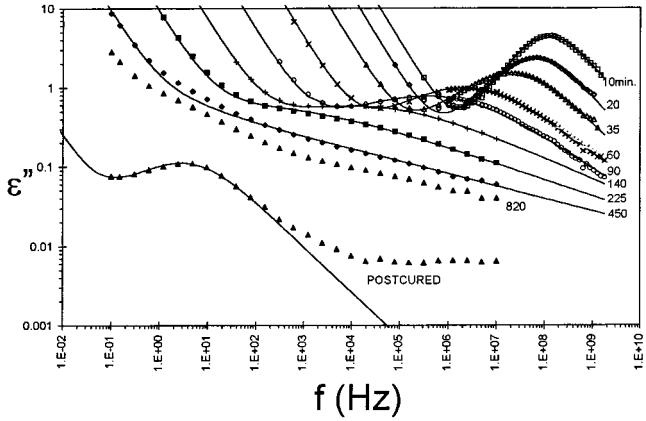

Figure 14. Dielectric loss spectra during isothermal reaction at 100 °C. Solid lines are fits to the Jonscher model, eq 5. The postcured sample was heated to 225 °C for 20 min (to maximize conversion of cyanate groups) and then cooled at 10 °C/min to the measurement temperature of 100 °C.

Many of the material properties derivable from a DRS experiment are of interest here, in terms of how they are influenced by the growth of a rigid network. We will discuss the real-time changes in conductivity, relaxation

Table 4. Relaxation Parameters (HN and Jonscher) for Samples at Selected Times during Isothermal Reaction at 110 °C

	Jonsher parameters					HN parameters			
min rxn	σ (1/Ω·cm)	$\Delta\epsilon_J$	τ_J (s)	m	n	$\Delta\epsilon_{HN}$	τ_{HN} (s)	a	b
10	5.30e−6[a]	8.82	1.47e−9	0.80	0.69	8.81	1.43e−9	0.80	0.87
20	1.99e−6	4.67	2.28e−9	0.62	0.68	4.98	3.16e−9	0.83	0.98
35	4.88e−7	2.99	6.30e−9	0.44	0.58	5.01	1.05e−8	0.60	0.98
60	5.96e−8	1.95	4.99e−8	0.33	0.45	4.91	5.65e−8	0.45	1.18
90	7.33e−9	1.47	1.43e−7	0.21	0.40	4.35	7.46e−7	0.43	0.98
140	9.79e−10	1.14	5.98e−6	0.18	0.26	4.36	2.05e−5	0.33	1.00
225	1.22e−10	1.09	1.09e−3	0.18	0.20	4.36	1.02e−3	0.30	1.00
postcure	3.22e−14	0.22	3.45e−2	0.37	0.57	0.44	3.72e−2	0.60	0.98

[a] Read as 5.30×10^{-6}.

strength, relaxation time, and relaxation shape. First we compare the conductivity and relaxation strength changes. Conductivity is obtained from a fit of $\sigma/(\omega\epsilon_v)$ to the low-frequency loss,[10] where σ is the dc conductivity, ω is the frequency in radians, and ϵ_v is the vacuum permittivity. The relaxation strength is obtained by fitting the dielectric loss with the Jonscher model; the parameters are given in Table 4. Both of these material properties are apparently directly sensitive to the increasing conversion.

As it was not our interest to investigate in more detail the reaction kinetics of the catalyzed system, no attempt has been made to verify any chemical kinetics determined by changes in the above properties with another technique such as infrared or DSC.

Next we contrast the changes in rotational mode dynamics (α process) against a diffusion mode, conductivity (it may be considered as tracer diffusion), in the reacting network. There have been several recent investigations on whether rotational and translational dynamics are correlated at all temperatures or become decoupled under certain circumstances.[37] We are interested in exploring these lines for the following reasons. In a recent publication[38] we described an alternative path for glass formation beyond the conventional path of rapidly cooling an isostructural liquid into an amorphous solid state. The second glass-forming path being an isothermal chemical reaction in which the reaction products have a T_g higher than the reaction temperature. We term the two paths: isostructural temperature path and isothermal chemical path. A question arises whether the isothermal chemical path will result in a decoupling of rotational and translational relaxation modes. These quantities, in the form of shifted relaxation time ($K - \log(\tau)$, where K is a constant) and conductivity, σ, are presented as a function of isothermal reaction time in Figure 15A. Unfortunately, τ values at longer reaction times are not available, as mentioned above, due to increasing uncertainty in the frequency of the loss peak maximum, since the peak diminishes and broadens with reaction. Nevertheless, it is apparent that these quantities become decoupled after 100 min of reaction. This trend is in contrast to the agreement found in the *temperature* dependence of the same quantities of the unreacted 0% sample, shown in Figure 15B. Rheological measurements during this chemical reaction are indicated to check whether the divergence is due to macroscopic gel formation.

The shape of the relaxation broadens significantly during network formation. We have quantified the shape with the Jonscher relaxation model, eq 2. These values are posted in Table 4. Our interpretations of the broadening are given above with the quench/reheat sample discussion.

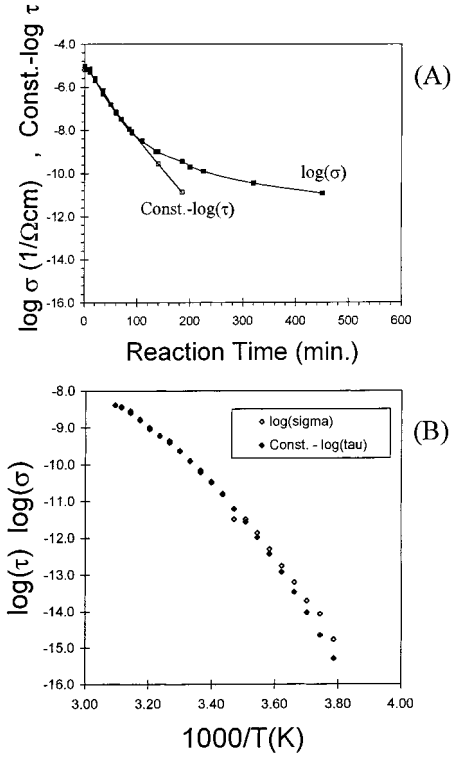

Figure 15. **(**A**)** Real-time changes in scaled τ and conductivity (σ) during network formation at 100 °C. **(**B**)** $1/T$ dependence of scaled log τ vs conductivity in the neat, 0% resin.

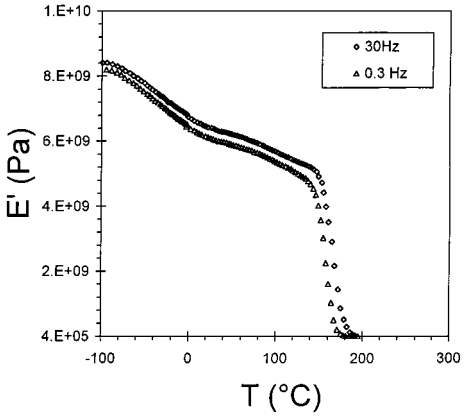

Figure 16. Bending modulus vs temperature at specified frequencies for a 95% cross-linked sample.

Rigid Network α Process: DMA and WAXS Studies. Dynamic Mechanical Analysis (DMA). To further probe the α process of a fully cured network, which clearly exhibits a calorimetric glass transition (cf. Figure 18), but whose severely broadened α process is not directly observable via DRS (we note that it is

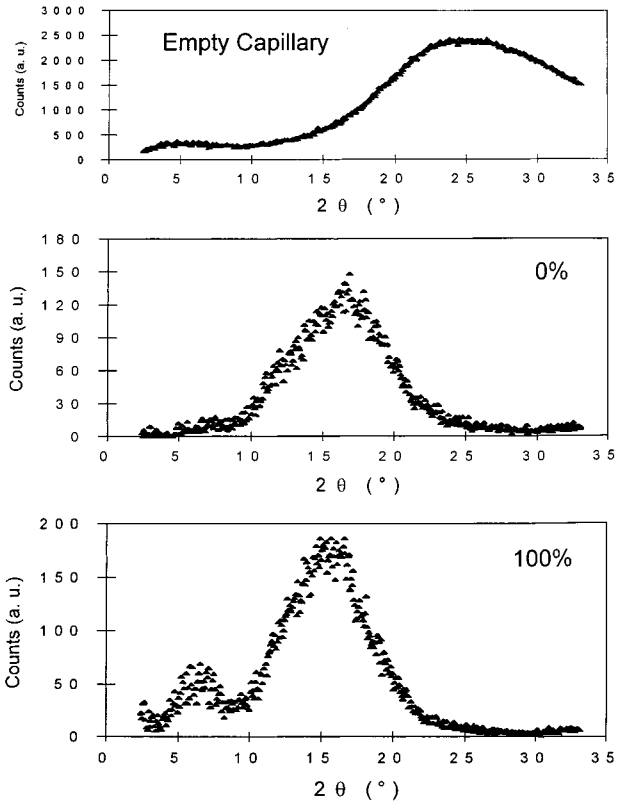

Figure 17. WAXS intensity vs 2θ for the 0 and 100% sample.

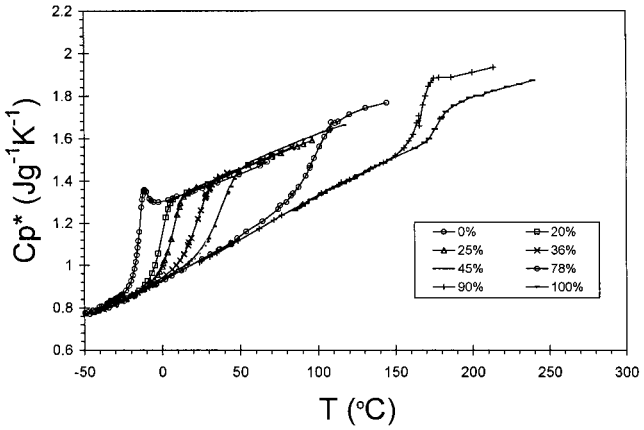

Figure 18. Relative heat capacity vs temperature for selected samples.

indirectly observable via changes in conductivity and dielectric constant in the glass transition temperature region), we employ DMA and wide-angle X-ray scattering.

Our DMA findings are presented first. A 95% reacted sample was scanned from −100 to 250 °C using 0.3, 1, 3, 10, and 30 Hz frequencies. The isochronal modulus is shown as a function of temperature in Figure 16. A low-temperature, sub-T_g, process is found. The activation energy of the sub-T_g process is 60 kcal/mol with a prefactor of $\ln \tau_0 = -110$. This process is not the same as the DRS measured β*, clearly the activation energy is far too large (∼3 times), and, additionally, the temperature range is different. This sub-T_g mechanical process remains unidentified. The activation energy of the α process is 170 kcal/mol with a prefactor of $\ln \tau_0 = -200$. The temperature range for the glass transition is in agreement with the DSC values, from 160 to 180 °C.

To probe whether any periodic three-dimensional structure exists in the network, a wide-angle X-ray scattering experiment was performed on the neat resin and the 100% network. The scattered intensity vs 2θ is given in Figure 17. In the neat resin there is a peak at 2θ of 17° (1.2 Å^{-1}), corresponding to an interparticle size of 6.5 Å (see below). In the 100% network there are two peaks, one at 16° (1.1 Å^{-1}) and another smaller peak at 6.5° (0.5 Å^{-1}); these peaks correspond to structures of approximately 17 and 7.2 Å, respectively. The size values are calculated from a well-known approximation that the amorphous liquid is composed of a random close-packed distribution of spheres.[39] Those assumptions lead to a length, d, where $d = 1.25(2\pi/q)$; q is the scattering vector defined by $q = 4\pi \sin(\theta)/\lambda$, λ is the X-ray wavelength, and 2θ is the detector angle. We interpret the ∼7 Å structure as intermolecular van der Waals contacts, while it seems plausible that the 17 Å structure in the 100% network is due to triazine network junctions. (As mentioned above, the average distance between triazines is ∼18 Å; cf. Figure 1.) These interesting findings call for further investigation.

Evaluation of the Feasibility of Monitoring of Cyanate Reaction via Permittivity Decay. Although the reaction product is a symmetric nonpolar triazine ring, it has been shown above that there is a contribution from this moiety to the overall permittivity. But at all conversions this contribution is much less than that from −O−C≡N dipoles, so that the relaxation strength is, to a good approximation, directly proportional to the −O−C≡N dipole concentration. Next, we make a further approximation, that the Onsager equation[40] yields reasonable values for the dielectric relaxation strength. It is reasonable to assume that, during reaction of the cyanate ester monomer, $\langle\mu^2\rangle$ for the unreacted −O−C≡N groups does not change. In this case we may use the Onsager equation to obtain N, the concentration of −O−C≡N dipoles (i.e., from a permittivity measurement, one may obtain the extent of reaction).

There are several experimental difficulties surrounding this idea. Foremost is the problem of obtaining an accurate determination of ϵ_0 and ϵ_∞. Inaccuracies in ϵ_0 may arise from low-frequency conductivity and electrode blocking effects,[41] while ϵ_∞ has two difficulties of its own: (1) instrumentation frequency limits (ϵ_∞ should be verified at frequencies up to ∼100 GHz, but our instrument is limited to 1.8 GHz), and (2) experimental artifacts from cables, resonance in the sample holder, and inevitable impedance mismatches at all connectors. In addition to these concerns are the difficulties in determining $\Delta\epsilon$ for α processes which are increasingly broad with cross-linking (cf. Figure 11). One solution for obtaining ϵ_∞ is to assume that it does not change significantly with temperature. One must then take a low-temperature approximation for ϵ_∞, namely, $\epsilon_\infty = \epsilon'$ measured at 10^6 Hz (or a suitably high frequency so as to avoid electrode or conductivity effects) at $T \ll T_\beta < T_g$. (For example, if T_g is 25 °C, use ϵ' at 10^6 Hz measured at −100 °C as one's approximation of the value for ϵ_∞ at all temperatures.) This approach may be valid if $\Delta\epsilon$ is >1 or if $\{\epsilon_\infty(\text{at } T \gg T_g) - \epsilon_\infty(\text{at } T \ll T_g)\} \ll \Delta\epsilon(T)$. For the cyanate ester system under investigation, the combined influences of electrode blocking effects and extreme broadening of the α process, and the appearance of the β* process at conversions higher than 65%, limit the foregoing procedure to evaluate conversion dielectrically, to conversions up to ∼50%.

Table 5. DSC Parameters for Samples at Selected Extents of Reaction

min rxn at 200 °C	T_g(DSC) (°C)	% rxn	ΔC_p* (J/g/K)	S_c*(0) (J/g K)	S_c*(∞) (J/g K)
0	−14	0	0.39	0.086	0.48
87	0	20	0.40	0.093	0.49
112	7	25	0.39	0.077	0.47
150	25	36	0.41	0.084	0.51
180	37	45	0.40	0.086	0.49
250	100	78	0.29	0.035	0.28
4[a]	164	90	0.28	0.031	0.32
24[a]	177	100	0.15	0.012	0.12

[a] In hours.

DSC: Configurational Entropy. We have obtained calorimetric data on samples of selected conversions. The samples were taken as aliquots from an uncatalyzed 200 °C reaction, and the results are summarized in Table 5. This table contains the reaction time, T_g (inflection point), ΔC_p [extrapolated C_p(liq) − C_p(glass)], slope and intercept of the C_p glass extrapolated line, and $S_c(0)$, $S_c(\infty)$ parameters. The last two parameters are derived from a recasting of the Adam−Gibbs (AG) model, ref 42, which was adapted by Alegria et al. in ref 43. We describe our use of the adaptation below. The AG model relates the configurational entropy (excess entropy of the material at a given temperature vs the extrapolated glass line) to the relaxation time. Figure 18 illustrates the C_p temperature dependence of the neat resin, the extrapolated C_p glass line, and the $\Delta C_p(T_g)$.

A small structural relaxation endothermic peak is seen just above the glass transition temperature. The C_p data for samples at selected conversion are given in Figure 18. The various conversions are referred to by their respective glass transition temperatures in this figure. In addition to the increasing T_g with conversion, there is an apparent constancy of $\Delta C_p(T_g)$ (see Table 5) for samples up to conversions of 45%. Such a trend is at variance with the ΔC_p behavior of an epoxide−amine cross-linking system[17,44] where the ΔC_p decreases linearly with conversion. We have used the data in Figure 18 to calculate the configurational entropy, S_c, for these samples. We take the configurational entropy to be the entropy difference of the measured liquid over that of the extrapolated glass. From thermodynamics, the configurational entropy of the supercooled liquid is defined as

$$S_c = S - S_g = \int_0^T \frac{C_p - C_{pg}}{T}\,dT - \Delta S_0 + \Delta S_f|_{T=0} = \int_0^T \frac{C_p - C_{pg}}{T}\,dT + S_c(0) \quad (9)$$

where S and S_g are the entropy of the supercooled liquid and glass, C_p and C_{pg} are the heat capacities of the supercooled liquid and glass, ΔS_0 is the glass-crystal entropy difference at 0 K, and ΔS_f is the entropy of fusion. We were not able to obtain ΔS_f because the cross-linked resin and neat monomer are not crystallizable. Instead, we lump that term together with the glass-crystal entropy into the $S_c(0)$ term. Our calculation of this term is given below.

Alegria et al.,[43] using an Adam−Gibbs argument, show that the configurational entropy may be derived from dielectric relaxation data in conjunction with calorimetric data, where

$$S_c = S_{liq} - S_{glass} = \Delta C_p(T_g) T_g \frac{T - T_v}{T T_v} \quad (10)$$

The T_v is obtained from a VFT fit of the temperature dependence of the dielectric relaxation time, while the $\Delta C_p(T_g)$ and T_g are taken from calorimetric data. As discusssed in the DRS sections above, we have obtained the T_v for samples up to 60% conversion; for all higher conversion samples, due to the complexity in the DRS response, $T_v = T_g - 60$ K was assumed. With the use of the $\Delta C_p(T)$ and T_g from the calorimetric experiments, we calculate ΔS_c, which according to our method of calculations vanishes at T_g. (Recall that we are taking the difference between the C_p(measured) and extrapolated C_p(glass), which are equal below T_g.) However, it is well-known that an excess configurational entropy exists below T_g[45] and is usually found for crystallizable liquids, since an account is able to be made for ΔS_f.[46−50] Since we cannot acquire this quantity, we must approximate by adjusting the DSC obtained S_c by the addition of a constant value, $S_c(0)$, given in Table 5, by best fitting the DSC S_c region $T_g + 10$ K $< T < T_g + 60$ K to the Alegria model of eq 7. A very good agreement is found between the vertically shifted calorimetric values and the model of eq 7, as shown in Figure 19.

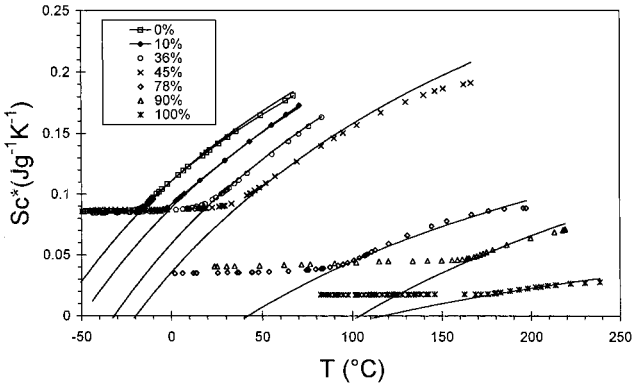

Figure 19. Configurational entropy vs temperature for samples at selected extents of cross-linking. The solid lines are generated from eq 10.

One notices in Figure 19 a lack of a change in $S_c(0)$ for samples up to 45%. This is directly related to the constancy of $\Delta C_p(T_g)$ with conversion up to 60%. Also of interest in Figure 19 are the changes with conversion of $S_c(0)$ and S_∞, as well as $S_0 - S_\infty$. The decrease of S_∞ and $S_c(0)$ is related to the fact that there is not a large difference between the structure of the liquid in the glassy and rubbery states, since the translational mobility is severely restricted by cross-links, and thus the ΔC_p is also decreasing after the gel point. We are interested in a comparison between the S_c values obtained with DRS and DSC. The DRS values of S_c are obtained from the Adam−Gibbs model in the form

$$S_c = \frac{S_\infty B}{T(\log \tau - \log \tau_0)} \quad (11)$$

where τ is obtained from a DRS measurement; B and τ_0 are determined from a VFT fit of the dielectric τ data, and S_∞ is the high-temperature limit of eq 11, $\Delta C_p(T_g)$-$*T_g/T_v$. A good agreement is found between DSC generated S_c and DRS generated S_c as shown in Figure 20.

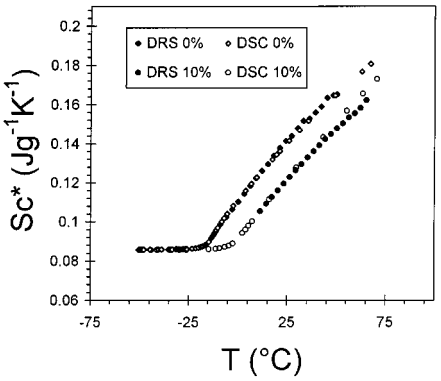

Figure 20. DRS vs DSC generated S_c as a function of temperature for two selected samples.

The agreement lends support to the AG heterogeneous model. We point out that despite the accumulating evidence for the heterogeneous description, the heterogeneous/homogeneous viewpoints continue to be intensely debated.[51]

Conclusions

In this rigid network-forming system the α process, when measured via DRS, broadens with cross-linking to the point that it is no longer identifiable. It has been argued that the increasing spanning of the cooperative domain by rigid network structures is the cause for the extreme broadening. Calorimetric and mechanical measurements are not sensitive to the extreme broadening. These techniques appear to probe a much larger length scale. The details of the differences in probed length scale between the techniques remain poorly understood.

It has been demonstrated that in-situ monitoring of the network-forming reaction via DRS is possible up to the gel point, approximately 60% conversion.

An unexpected secondary relaxation process, β*, is found. Model compounds and conformational strain analysis have suggested a likely molecular mechanism.

The α process in selected cyanate networks was analyzed with the Adam−Gibbs thermodynamics-based relations (AG model).[42] The AG model provides a link between the relaxation time of a cooperatively rearranging domain (CRD) and configurational entropy. The model was explored via DRS and calorimetrically for various network structures. A reasonable agreement is found between quantities derived from both techniques when examined in the AG framework. These results lend support to the CRD concept used in the AG model and, more generally, toward the establishment of the heterogeneous view of relaxations in glass-formers.

The cyanate materials studied here find use as insulating thermoset materials and are prized for their low dielectric constants (compared with alternative thermosets). The forethinking behind the choice of monomer is based on the lack of polarity in the units between the cross-link sites and the symmetry (and therefore low polarity) of the triazine network nodes. We have shown here that this polymeric network has an unusual secondary β process, which at application/use temperatures (up to ∼80 °C) is not active. This implies that for the fully reacted material, from low temperature up to 80 °C, the dielectric constant of the material (this is the design parameter intended to be minimized by judicious monomer choice and chemistry) is ϵ'_∞ (cf. eq 2). This means that the important contributions to the dielectric constant are atomic and electronic polarizability, which depend on quantum mechanical factors and not on the polarity of the groups present (since there will be no reorientational contributions from these groups under the present conditions). This is true for any insulating thermoset; however, other thermosets such as epoxy/amines have been shown to have a "usual" β process, and under application/use temperatures this process is active and thus presents polar reorientational contributions to the overall polarization.

Acknowledgment. This material is based on work supported by the National Science Foundation under Grants DMR-9710480 and INT-9724714. We are grateful to Professors Francesco Bellucci, Jose Kenny, and Iñaki Mondragon for helpful discussions.

References and Notes

(1) Hammerton, I. *Chemistry and Technology of Cyanate Ester Resins*; Blackie Academic and Professional: Berlin, 1994.
(2) Deutch, A.; Surovic, C.; Lanzetta, A.; Ainspan, H.; Abbiate, J.; Viehbeck, A.; Hedrick, A. *IEEE Trans. Comput.* **1996**, *19*, 331.
(3) Körner, H.; Shiota, A.; Bunning, T.; Ober, C. *Science* **1996**, *272*, 252.
(4) Fitz, B.; Mijovic, J. *Macromolecules* **1999**, *32*, 3518.
(5) Deng, Y.; Martin, G. *Polymer* **1996**, *37*, 3593.
(6) Fyfe, C.; Niu, J.; Rettig, S.; Burlinson, N.; Reidsema, C.; Wang, D.; Polkis, M. *Macromolecules* **1992**, *25*, 6289.
(7) Simon, S.; Gillham, J. *J. Appl. Polym. Sci.* **1993**, *47*, 461.
(8) Flory, P. *Principles Of Polymer Chemistry*; Cornell University Press: Ithaca, NY, 1953.
(9) Bauer, J.; Lang, P.; Burchard, W.; Bauer, M. *Macromolecules* **1991**, *24*, 2634.
(10) McCrum, N. G.; Read, B.; Williams, G. *Anelastic And Dielectric Effects In Polymeric Solids*; Wiley: New York, 1967.
(11) Fröhlich, H. *Theory Of Dielectrics*, 2nd ed.; Oxford University Press: Oxford, 1958.
(12) Williams, G.; Watts, D. C. *Trans. Faraday Soc.* **1970**, *66*, 80. Kohlrausch, R. *Ann. Phys.* (*Leipzig*) **1847**, *12*, 393.
(13) Havrilliak, S.; Negami, S. *J. Polym. Sci., Part C* **1966**, *14*, 99.
(14) Jonscher, A. *Dielectric Relaxation In Solids*; Chelsea Dielectric Press: London, 1983.
(15) Dissado, L.; Hill, R. *Nature* **1979**, *279*, 685.
(16) Simon, S.; Gillham, J. *J. Appl. Polym. Sci.* **1994**, *51*, 1741.
(17) Venditti, R.; Gillham, J. *J. Appl. Polym. Sci.* **1997**, *64*, 3.
(18) Fitz, B.; Andjelic, S.; Mijovic, J. *Macromolecules* **1997**, *30*, 5227.
(19) Chiu, S. C., private communication.
(20) Sillescu, H. *J. Non-Cryst. Solids* **1999**, *243*, 81.
(21) Johari, G. P.; Goldstein, M. *J. Chem. Phys.* **1970**, *53*, 2372.
(22) Nakagawa, K.; Ishida, Y. *J. Polym. Sci., Polym. Phys.* **1973**, *11*, 1503.
(23) Graff, M.; Boyd, R. *Polymer* **1994**, *35*, 1797.
(24) Glatz-Reichenback, J.; Sorriero, L.; Fitzgerald, J. *Macromolecules* **1994**, *27*, 1338.
(25) Roland, C. *Macromolecules* **1994**, *27*, 4242.
(26) Schlosser, E. *Plaste Kautschuk* **1968**, *15*, 652.
(27) Cassalini, R.; Livi, A.; Rolla, P.; Levita, G.; Fioretto, D. *Phys. Rev. B* **1996**, *53*, 564.
(28) Andjelic, S.; Fitz, B.; Mijovic, J. *Macromolecules* **1997**, *30*, 5239.
(29) Schlosser, E.; Schönhals, A. *Colloid Polym. Sci.* **1989**, *267*, 133.
(30) Tabbelout, M.; Randrianantoandro, H.; Emery, J.; Durrand, D.; Hayward, D.; Pethrick, R. *Polym. Pap.* **1995**, *36*, 4547.
(31) Katana, G.; Kremer, F.; Fischer, E.; Plaetschke, R. *Macromolecules* **1993**, *26*, 3075.
(32) Kumar, S.; Colby, R.; Spiros, A.; Fytas, G. *J. Chem. Phys.* **1996**, *105*, 3777.
(33) Ngai, K. L.; Roland, M. C. *Macromolecules* **1993**, *26*, 6824.
(34) Vogel, H. *Phys. Z.* **1921**, *22*, 645. Fulcher, G. *J. Am. Ceram. Soc.* **1923**, *8*, 339. Tamman, G.; Hesse, W. *Anorg. Allg. Chem.* **1926**, *156*, 245.
(35) At this stage of conversion we have qualitatively confirmed that a macroscopic gel has formed by prodding the reaction test tube contents with a stirring rod.

(36) Angell, C. A. In *Relaxations in Complex Systems*; Ngai, K. L., Wright, G., Eds.; National Technical Information Service, U.S. Department of Commerce: Springfield, VA, 1984.
(37) (a) Rössler, E. *Phys. Rev. Lett.* **1990**, *65*, 1595. (b) Blackburn, F.; Cicerone, M.; Hietpas, G.; Wagner, P.; Eidiger, M. *J. Noncryst. Solids* **1994**, *172−174*, 256. (c) Hansen, C.; Stickel, F.; Richert, R.; Fischer, E. *J. Chem. Phys.* **1998**, *108*, 6408.
(38) Fitz, B.; Mijovic, J. *Macromolecules* **1999**, *32*, 4134.
(39) Klug, H. P.; Alexander, L. E. *X-ray Diffraction Procedures*; Wiley: New York, 1974.
(40) Onsager, L. *J. Am. Chem. Soc.* **1936**, *58*, 1486.
(41) Senturia, S.; Sheppard, N. *Adv. Polym. Sci.* **1986**, *80*, 1.
(42) Adam, G.; Gibbs, J. *J. Chem. Phys.* **1965**, *43*, 139.
(43) Alegria, A.; Guerrica-Echevarria, E.; Goitiandia, L.; Telleria, I.; Colmenero, J. *Macromolecules* **1995**, *28*, 1516.
(44) Wang, X. J. *Appl. Polym. Sci.* **1997**, *64*, 69.
(45) Kauzmann, W. *Chem. Rev.* **1948**, *43*, 219.
(46) Magill, J. *J. Chem. Phys.* **1967**, *47*, 2802.
(47) Chang, S.; Bestul, A. *J. Chem. Phys.* **1972**, *56*, 503.
(48) Takahara, S.; Yamamuro, O.; Matsuo, T. *J. Phys. Chem.* **1995**, *99*, 9589.
(49) Naoki, M.; Seki, M.; Kugo, H.; Saito, F.; Tanioka, T. *J. Phys. Chem.* **1991**, *95*, 5628.
(50) Richert, R.; Angell, C. A. *J. Chem. Phys.* **1998**, *108*, 9016.
(51) *Heterogeneous view* [multi-D NMR]: Heuer, A.; Spiess, H. *Phys. Rev. Lett.* **1999**, *82*, 1335. *Homogeneous view* [incoherent neutron scattering]: Arbe, A.; Colmenero, J.; Monkenbusch, M.; Richter, R. *Phys. Rev. Lett.* **1999**, *82*, 1336.

MA9911243